LASER INTERFEROMETER GRAVITATIONAL WAVE OBSERVATORY
-LIGO-
CALIFORNIA INSTITUTE OF TECHNOLOGY
MASSACHUSETTS INSTITUTE OF TECHNOLOGY

Technical Note **LIGO-T070026- 01- W** 22 May 2007

Status of the LIGO photon calibrators: February 2007

Evan Goetz, Peter Kalmus, Rick Savage

DRAFT

California Institute of Technology
LIGO Project - MS 18-34
Pasadena CA 91125
Phone (626) 395-2129
Fax (626) 304-9834
E-mail: info@ligo.caltech.edu

Massachusetts Institute of Technology
LIGO Project - MS NW17-161
Cambridge, MA 02139
Phone (617) 253-4824
Fax (617) 253-4824
E-mail: info@ligo.mit.edu

WWW: http://www.ligo.caltech.edu/

Contents

1 Introduction

This document describes the measurements we have made using the photon calibrator. We also discuss investigations to understand the differences between using the "official" calibration method and the photon calibrator to calibrate the end test mass (ETM) coil actuators.

2 Principle of operation

A single photon of frequency ν carries momentum p

$$p = \frac{h\nu}{c} \tag{1}$$

where h is Planck's constant and c is the speed of light. If the photon reflects with angle of incidence θ from the surface of a macroscopic object (such as an ETM), it transfers momentum

$$p_{refl} = 2p\cos\theta \tag{2}$$

to the object where p_{refl} is the transferred momentum. Suppose that there are n such photons per second with energy $h\nu$, then a force $F(t)$ will be produced

$$F(t) = \frac{dp_{refl}}{dt} = \frac{2\cos\theta}{c}\frac{d\left(h\nu n\right)}{dt} = \frac{2\cos\theta}{c}P(t), \tag{3}$$

where $P(t)$ is the power of a stream of photons as a function of time.

During the calibration procedure we want modulate the power to drive the test mass sinusoidally, so the total power may be expressed as a sinusoidal power

$$P(\omega, t) = P_{dc} + P_0 e^{i\omega t}, \tag{4}$$

where ω is the angular frequency of the beam power modulation, P_{dc} is the DC offset and it pushes the test mass with a constant force, and P_0 is amplitude of the power modulation.

If the suspended test mass is treated as a simple pendulum, its equation of motion is given by

$$\frac{F(\omega, t)}{M} = \frac{2\cos\theta}{Mc}P_0 e^{i\omega t} = \ddot{x}(\omega, t) + \gamma\dot{x}(\omega, t) + \omega_0^2 x(\omega, t) \tag{5}$$

where M is the mass of the test mass, γ is the velocity dependent damping coefficient, and $\omega_0^2 = g/l$ is the resonant frequency ($\omega_0 = 2\pi f_0$) with g is the acceleration of gravity and l is the length of the pendulum suspended mass.

The the complex amplitude of the sinusoidal motion ($x(\omega, t) = x_0 e^{i\omega t}$) in response to the sinusoidally modulated force is given by

$$x_0(\omega) = \frac{2P_0\cos\theta}{Mc}\frac{1}{\omega_0^2 - \omega^2 + i\omega\omega_0/Q} \tag{6}$$

where $Q = \omega_0/\gamma$ is the quality factor.

If the frequency of modulation of the beam is much higher than the resonance frequency of the pendulum, $\omega \gg \omega_0$, then Equation 6 reduces to

$$x_0(\omega) \simeq -\frac{2P_0\cos\theta}{Mc\omega^2}. \tag{7}$$

In the case of the photon calibrator, $f_0 \simeq 0.76$ Hz and $f \sim$ a few tens of Hz to a few kHz.

2.1 Correction due to beam mis-centering

There is a correction due to potentially uncentered main interferometer and photon calibrator beams. If the photon calibrator beam is not centered on the test mass, it will cause an angular motion of the test mass at frequency ω. If the main interferometer beam is perfectly centered there will be no net effect in the gravitational wave channel, to first order in the rotation angle, ϕ. However, if the main beam is not centered, the interferometer will interpret the angular motion as a longitudinal length change.

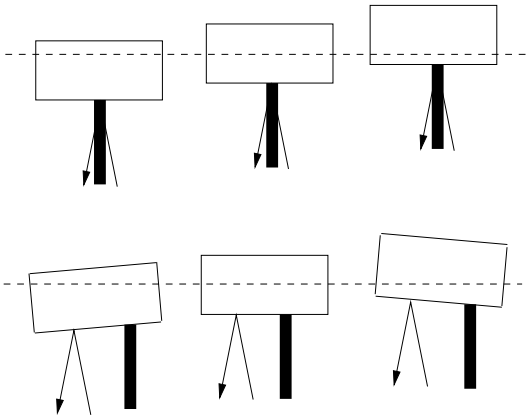

Figure 1: The top images show the ETM motion if both the photon calibrator and interferometer beam are centered. If the photon calibrator and interferometer beams are not aligned, as in the bottom images, then there is an induced rotation which is either in-phase or out of phase with the pendulum motion.

Let us assume, as before, that the frequency modulation of the power is much greater than the pendulum and rotational resonant frequencies of the suspended test mass. Then we could write,

$$M\ddot{x}(\omega,t) = F(\omega,t) \tag{8}$$
$$I\ddot{\phi}(\omega,t) = aF(\omega,t). \tag{9}$$

where I is the rotational inertia of a right circular cylinder about an axis through the center of mass perpendicular to the circular surface, ϕ is the rotation angle, and a is the distance away from the axis of rotation the photon calibrator beam is aligned. Solving these differential equations, we have for the displacement of the center of mass

$$-\omega^2 M x_0(\omega) = \frac{2P_0\cos\theta}{c} \tag{10}$$
$$x_0(\omega) = -\frac{2P_0\cos\theta}{Mc\omega^2} \tag{11}$$

as before, and the angular rotation,

$$-\omega^2 I\phi_0(\omega) = \frac{2P_0 a\cos\theta}{c} \tag{12}$$
$$\phi_0(\omega) = -\frac{2P_0 a\cos\theta}{Ic\omega^2}. \tag{13}$$

The rotation of the test mass will be sensed by the interferometer if the interferometer beam is also displaced from the axis of rotation. If the interferometer beam is displaced by a distance b, then the interferometer cavity will lengthen by a factor

$$x_\phi(\omega) = b\sin\phi \simeq b\phi = -\frac{2P_0 ab\cos\theta}{Ic\omega^2} \tag{14}$$

Then the actual displacement due to motion of the center of mass and that due to rotation is

$$x' = x_0 + x_\phi = -\frac{2P_0\cos\theta}{Mc\omega^2}\left(1+\frac{abM}{I}\right). \tag{15}$$

Figure 2 plots the bracketed term in Equation 15 for a variety of beam offsets.

Assuming a well centered photon calibrator beam, or interferometer beam, $abM/I \simeq 0$. It has been shown here that with proper knowledge of the modulated power amplitude, P_0, and ETM mass, M, the displacement of an ETM can be calculated. This displacement amplitude is critical in understanding the response of the interferometer.

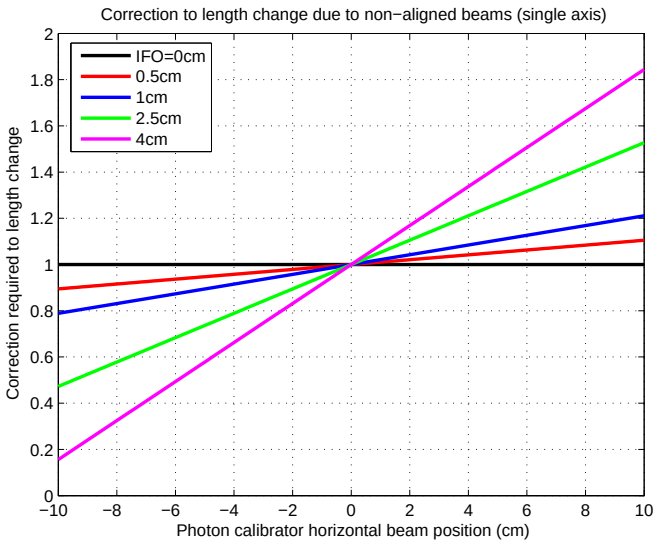

Figure 2: The theoretical prediction of the correction factor $1 + abM/I$ for various interferometer beam offsets as a function of photon calibrator beam offset.

3 Experimental setup

Two photon calibrator units are mounted on each of the three LIGO interferometers, one near each ETM (Figure 3). The laser of each photon calibrator is aimed at the ETM reflective surface. Either photon calibrator can be used to measure the response function of a given interferometer, but one on each ETM is necessary to reduce the errors when calibrating the coils because differences in the mass of the mirrors will introduce an error unless the mass is well known.

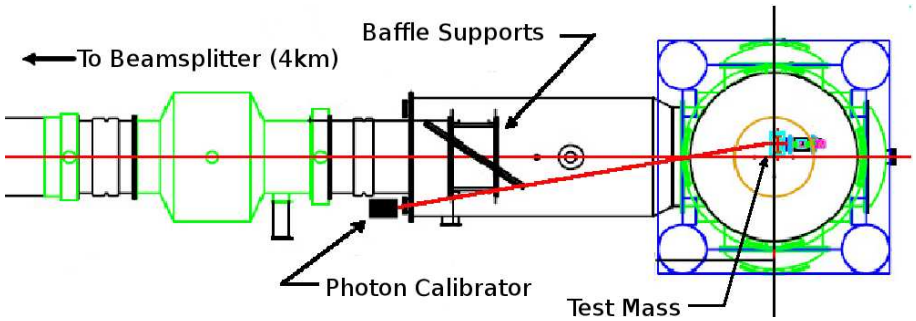

Figure 3: Top view of photon calibrator enclosure mounted near an end test mass. A beam enters the vacuum chamber through a glass viewport and is aimed as close to the center of the test mass as possible to avoid inducing torque on the test mass. In the case of the Hanford 4 km detector (shown here) the beam must pass between two vertical baffle supports and is misaligned from the center of mass.

The major components of the system (see Table 1) are a ~ 500 mW 1047 nm Nd:YLF laser; an acousto-optic modulator (AOM) which modulates the laser beam power; and a photodetector (photodiode) which monitors a small fraction ($\sim$1%) of the beam power transmitted by a partially reflecting mirror. Monitoring of the sample beam allows for a calculation of the output power of the system. Once we know the power modulation, we can calculate the expected test mass displacement.

The arbitrary waveform generator (AWG) sends signals to the photon calibrator input through an ICS 110B digital to analog converter. This drives our AOM after passing through filtering electronics. The photodiode within the photon calibrator sends an analog signal (after passing through filtering electronics) to a Pentek analog to digital converter which samples the signal at a data rate of 16384 Hz.

Table 1: Major components of the system.

Item	Notes	Vendor	Model No.
Laser	500mW 1047nm Nd:YLF	CrystaLaser	IRCL-500-1047
AOM	30MHz bandwidth	Isomet	1205C-843
AOM Driver	80MHz center freq.	Isomet	232A-1
Photodetector	5-mm Ge	New Focus	2033

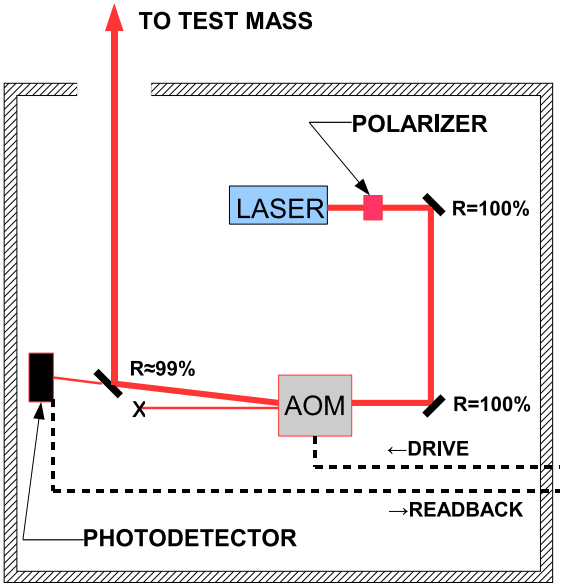

Figure 4: Schematic layout of a photon calibrator optical table showing major components of the system. This optical table is installed inside the enclosure which is mounted as shown in Fig. 3. The beam passes through a polarizer and the AOM before being emitted from the enclosure, through the viewport into the vacuum system and onto the test mass. A small fraction of the beam is continuously picked off for readback by the photodetector, so that power incident onto the test mass can be estimated.

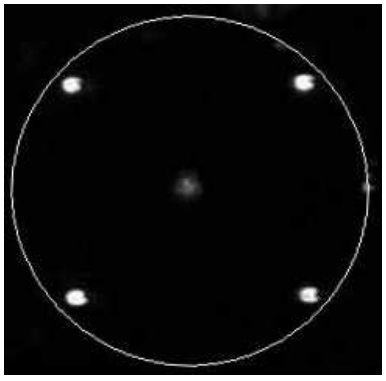

Figure 5: Photo of an end test mass, suspended *in situ*, with a photon calibrator beam visible at the center. The 4 spots near the edge of the test mass mark the locations of the coil actuators. The white circle marks the approximate edge of the test mass. Spacing between adjacent coil actuators is about 16 cm, and test mass diameter is about 25 cm.

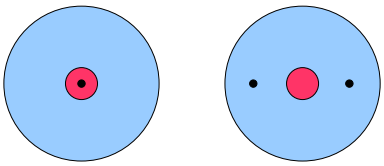

Figure 6: Schematic diagrams of single beam (left) and split beam (right) photon calibrator setups, showing the main interferometer beam in red and the photon calibrator beam(s) in black incident on a test mass.

3.1 DC photodetector calibration

The calibration of the photodetector within the photon calibrator is critical in obtaining a correct calibration of the interferometer. This calibration factor is proportional to the power reflecting off of the optic, P_{optic}, where

$$P_{optic} = (T_{VP})\,(R_{TM})\,P_{box} \tag{16}$$

where the two multiplicative factors, viewport transmission T_{VP} and test mass reflectivity R_{TM} are slightly less than 1, and it is assumed that there is no other power loss between the enclosure and the optic. P_{box} is the power emerging from the enclosure, and it can be written in terms photodetector readout channel:

$$P_{box} = \alpha_c V_{PD} \tag{17}$$

where V_{PD} is the number of DAQ counts, or volts, returned by the photodetector readout channel, and α_c is a conversion factor in units of power per DAQ counts.

To measure α_c, a handheld power meter was placed in front of the beam immediately before it leaves the enclosure (LHO Ophir unit #4 with thermal head 10A). DAQ counts from the photodetector and the power (in mW) displayed by the power meter were recorded for several different DC voltage values to the AOM driver input. These measurements are made at DC; the transfer function between the input to the AOM driver and the beam power incident on the power meter is reasonably flat from DC up to ∼2 kHz (see Section 3.7). We plot the DAQ counts versus power and fit these values to a trendline (Figure 7). The slope of this line is the calibration factor, α_c, of the photodetector. For further discussion, see Appendix A.

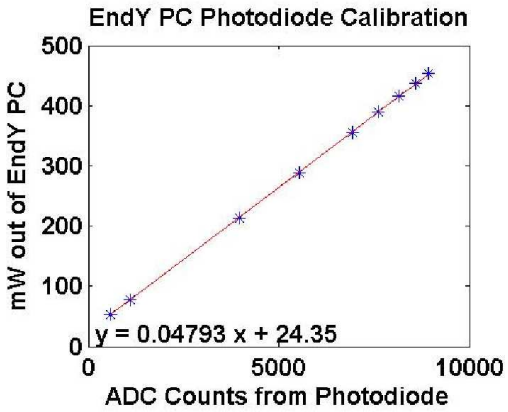

Figure 7: Example photodetector conversion factor (α_c) plot. Only the slope of the line is important, as measurements will always be peak-to-peak.

3.2 AC photodetector calibration

To make sure that the photodetector calibration is flat with frequency within our measurement band, we placed a mechanical chopper in front of the photodetector and connected the output of the photodetector to an oscilliscope. We rotated the chopper blade into the beam by hand, completely blocking the beam, and out of the beam, completely passing the laser beam. In each position, we set the cursor of the oscilliscope to the top of

the measurement noise that we see on the scope. For the scope setting we had of 32 mV per division and a full scale chopped photodetector voltage of 236 mV, the noise has a width of ∼5 mV (or 2 percent). The cursor has a much finer resolution, of course, so we believe that the settings are good to less than 1 percent.

Next, we set the chopper to rotate at a low frequency (∼ 5 Hz, Figure 8) and high frequency (∼ 370 Hz, Figure 9). At each frequency, we looked to see whether the peak-to-peak values reached each cursor. Notice that the low frequency and high frequency traces reach the cursor values, although the high frequency one looks slightly shifted because the structure of the noise is now visible due to the finer time resolution at high frequency.

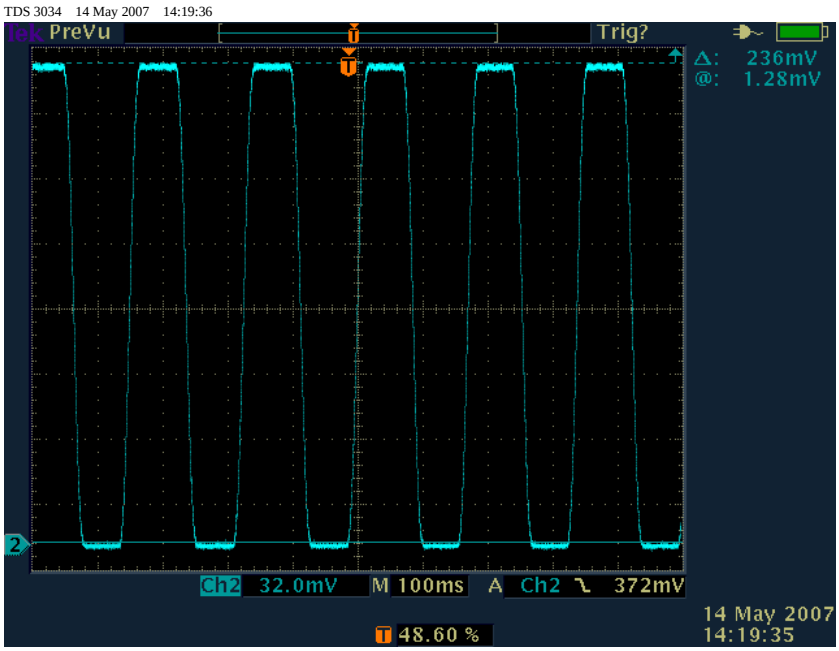

Figure 8: Low frequency response of PD

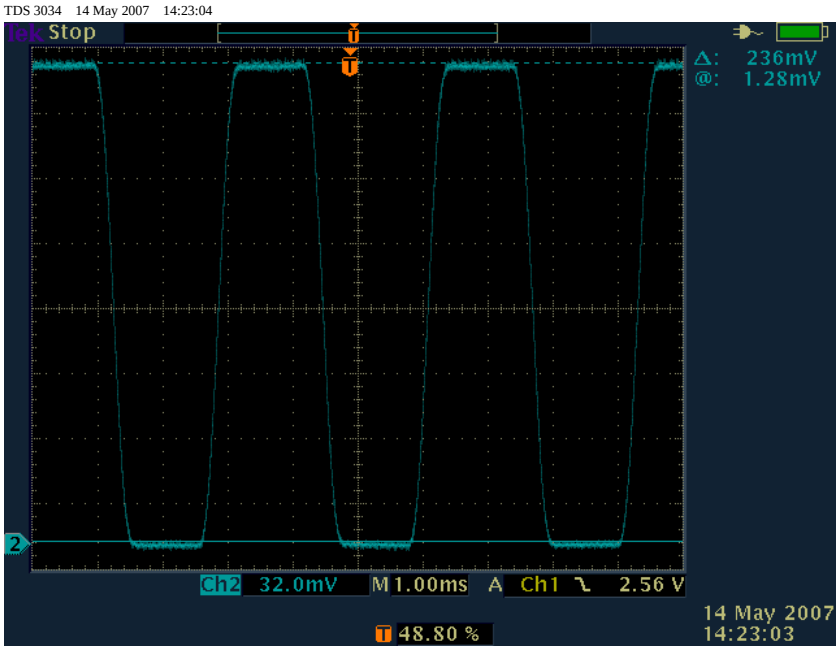

Figure 9: High frequency response of PD

3.3 Viewport reflection

The viewport reflects a small portion of the incident beam, reducing the total power reaching the ETM. We assume that there is negligable absorption due to the viewport. We measure the incident and reflected power from the viewport. The ratio of these powers gives the reflection coefficient ($R_{VP} = 1 - T_{VP}$). The results for each ETM viewport are given in Table 2. When using the Ophir PD300 head, it is important to have the right wavelength setting on the power meter. The calibration difference between 1064 nm and 1047 nm is a factor of about 0.8.

Table 2: Viewport reflectivities for the six photon calibrator units' viewports.

Viewport	**H1X**	**H1Y**	**H2X**	**H2Y**	**L1X**	**L1Y**
Reflectivity (%)	7.1	1.1	1.1	0.8	7.2	7.2

3.4 ETM reflection

Photons which reflect off of the ETM transfer twice their momentum to the ETM (Section 2). It is necessary to measure the reflection coefficient of the ETMs. This is a difficult measurement and we have tried two methods to measure this.

The first measurement involves using the witness plates of the ETMs in the lab. We measure the reflection coefficient at the working angle of incidence of nine degrees. This incidence angle is the same as that on the interferometers. The results are given below. Here we have assumed that the witness plates have the same reflection properties as the ETMs in the vacuum enclosure of the interferometers. In the lab, we find the witness plate for the ETMs reflect 99.97 percent of the incident power.

The second measurement uses the actual ETM in the vacuum enclosure. We aligned a photon calibrator laser beam to reflect off the ETM and exit another viewport by sending the beam in through an optical lever laser viewport (see LHO elog from 10 October 2006 and 22 December 2006). We measured the power into and out of the vacuum enclosure. Then we measured the reflection coefficients of the input and output viewports using the method described in the previous section. These results confirm our lab measurements to within 2 percent. **The unaccounted 2 percent may be accounted for by using a silicon head power meter with 1047 nm dialed in as the incident laser.** This measurement also confirms our assumption that there are no large losses of power to the ETM (within 2 percent). See Appendix C for further details.

3.5 Angle of incidence

To estimate the angle of incidence of the photon calibrator laser beam on the ETMs, we used AutoCad drawings of the location of the photon calibrator in relation to the estimated ETM position in the chambers. For H1, H2 and L1, we estimate the angle of incidence to be 9.6 degrees. We determine this from the geometrical factors in the as-built drawings.

Table 3: Values from the as-build drawings to determine the angle of incidence for the photon calibrators.

Parameter	**Value**
Transverse horizontal distance	0.96 m
Transverse vertical distance	0.049 m
Longitudinal distance from input surface of Pcal viewport to ETM surface	5.723 m
Transverse distance in plane of incidence	0.96 m
Angle of incidence	9.6 degrees

3.6 ETM mass

Using measurements of the geometry of the ETMs and the density of the test mass substrate, we have estimated the mass of the ETMs from a Matlab script. These calculations were performed on an ITM which was removed from H1. The calculation and measurement of the mass agreed to better than 1 percent. See Appendix E for further details.

Table 4: ETM masses

H1X	H1Y	H2X	H2Y	L1X	L1Y
10.346 kg	10.388 kg	10.372 kg	10.363 kg	10.353 kg	10.365 kg

3.7 Electronics transfer function

The photodiode calibration is done at DC, but the photon calibrator operates in the range of a few tens of Hz to a few kHz. It is therefore necessary to understand how the calibration is effected at higher frequencies by measuring the transfer functions of the photon calibrator and associated electronics. Below are the results of the transfer function measurements made between 10 Hz and 100 kHz.

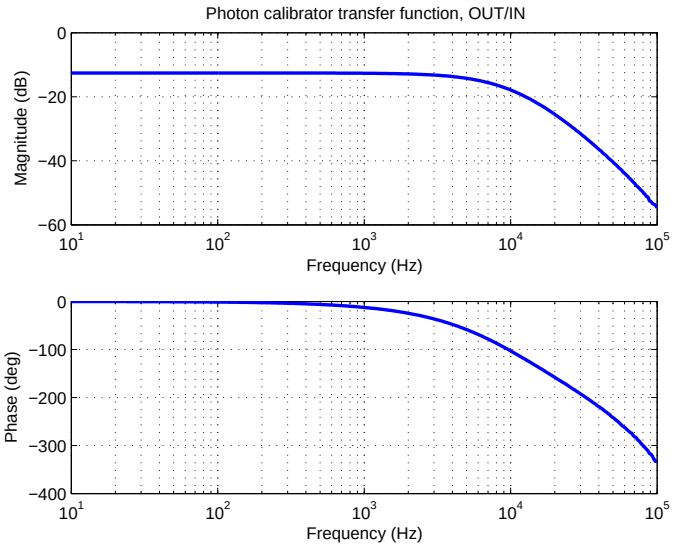

Figure 10: An example transfer function of a photon calibrator. An excitation is sent to the photon calibrator input and the readback to the DAQ is the output.

From Figure 10 we have determined that the photon calibrator drive and readback is flat to less than 1 percent at 1.6 kHz, our nominal S5 operating frequencies. The readback alone is flat to less than 1 percent, as shown in Figure 12. At high frequencies (> 2 kHz), the calibration of the photodiode (which is done effectively at DC) must be adjusted for the roll-off of the photodiode electronics.

3.8 Electronics cross-talk check

To make sure none of the excitation signal was cross-talking to the readback channel, we ran an excitation into the photon calibrator with the laser on, then off. We measured the transfer coefficient of the excitation with the laser on to be 1.47, and with the laser off we measured the transfer coefficient to be 5×10^{-7}. We conclude that there is no significant noise from cross-talking channels. (See LHO elog from 12 Dec 2006 by EG.)

3.9 Alignment of the photon calibrator beam

The photon calibrator beam is aligned to strike the ETM reflecting surface as near to the center of mass as possible (for the single beam configuration) or well balanced on either side of the center of mass (for the two beam configuration). We use the spool camera images to view the ETM as we scan the photon calibrator beam across the optic. In order to use the spool images to properly align the photon calibrator beam(s), we must account for the parallax from a camera which views the ETM at a horizontal angle of 5.1 degrees (LHO). At LLO, the horizontal angle is ?? and vertical angle is ??.

The OSEMs are used as a reference scale. The horizontal separation (center to center) is 6.364 inches, and the vertical separation is 6.354 inches. We also assume the OSEMs are 10 cm behind the front, reflecting,

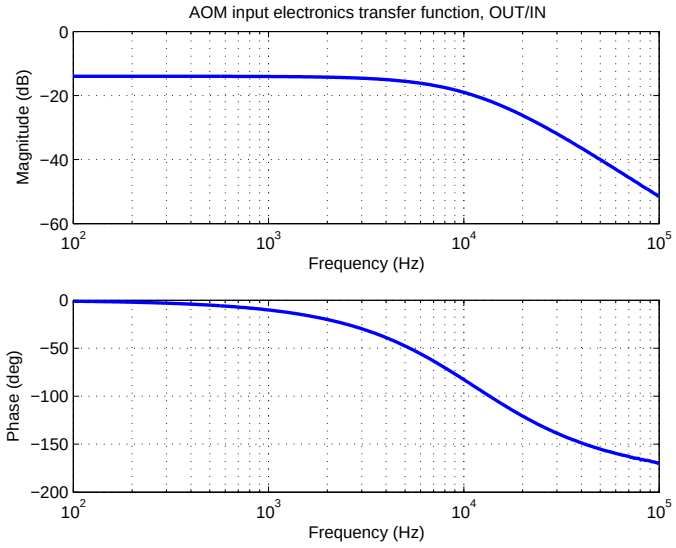

Figure 11: An example transfer function of the input AOM electoronics. An excitation is sent to the photon calibrator input and the signal to the AOM driver input is the output.

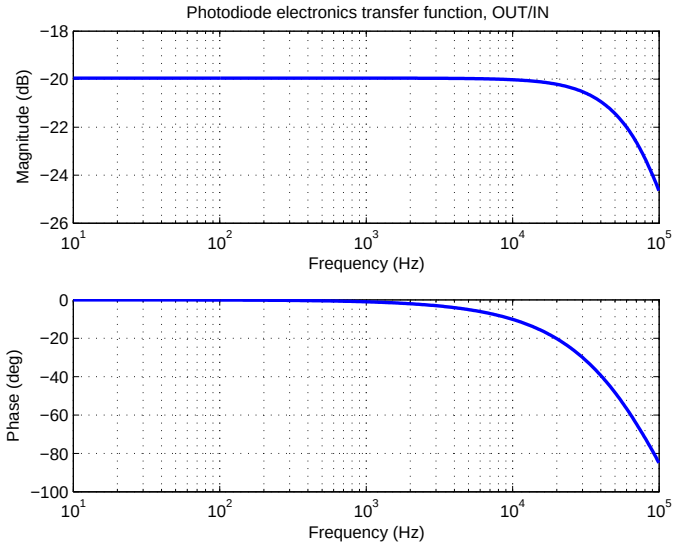

Figure 12: An example transfer function of the output photodiode electoronics. An excitation is sent to the photodiode electronics input and the signal to the DAQ is the output.

surface of the ETM. The index of refraction of the optical substrate is 1.45. Using Snell's Law,

$$n_1 \sin\theta_1 = n_2 \sin\theta_2, \tag{18}$$

$\theta_2 = 3.5$ degrees for LHO. For LLO the angles are ?? horizontally and ?? vertically.

At LHO, when viewing the ETM front surface from the left (as you face the reflecting surface), beams that are centered will appear to be 0.6 cm to the right. Therefore when attempting to center a photon calibrator beam using the spool image and OSEMs, the spot must appear slightly to the right. If the view is from the right instead of the left, then a well centered spot will appear 0.6 cm to the left of center of the OSEMs. At LLO, centered beams appear .....

For beams that are purposefully offset from center, the full equation is for an offset x is given by,

$$x = \frac{m}{\cos\theta_2} + d\tan\theta_2 \tag{19}$$

where m is the additional offset (in the same direction as the centered beam offset) viewed in the spool image, and $d = 10$ cm.

For L1 and H2, the center of the ETM is easily viewable from the currently assigned photon calibrator viewport. However, for H1, the center of the optic is partially occluded due to arm cavity baffle supports (and soon the baffles themselves will occlude the optic entirely!). Due to the baffle supports, Equation 19 is important for misaligned beams (see Section 2.1).

4 Measurements and results

4.1 Response function

The response of an interferometer to an external disturbance is determined by the gain of the DARM servo loop and the sensing function of the interferometer. Together these give the response function of the interferometer to an external disturbance.

To measure the response function with the photon calibrator, we inject into ifo:LSC-ETMi_CAL_EXC and read back the two channels ifo:LSC-DARM_ERR and ifo:LSC-ETMi_CAL, the latter being the photodetector read back channel. For an example, see Figure 13. The result of this measurement is then scaled by the expected motion of a free mass (Equation 15). See Figure 15. By scaling the transfer function, we directly measure $R(\omega, t)$.

The loop algebra for using the photon calibrator gives the transfer function,

$$\frac{\text{DARM\_ERR}}{\text{ETMX\_CAL}} = -\frac{\gamma(t)C(\omega,t_0)}{1+\gamma(t)G(\omega,t_0)} b_{\text{X}}\text{pendX} = -\frac{1}{R(\omega,t)} b_{\text{X}}\text{pendX} \tag{20}$$

for the X-arm photon calibrator and

$$\frac{\text{DARM\_ERR}}{\text{ETMY\_CAL}} = \frac{\gamma(t)C(\omega,t_0)}{1+\gamma(t)G(\omega,t_0)} b_{\text{Y}}\text{pendY} = \frac{1}{R(\omega,t)} b_{\text{Y}}\text{pendY} \tag{21}$$

for the Y-arm photon calibrator. In these transfer function equations, b_{X} and b_{Y} are the calibration of the photon calibrators at 1 Hz, $R(\omega, t)$ is the response function and pendX and pendY are the pendulum transfer functions which are essentially free mass transfer functions for $\omega \gg \omega_0$:

$$\text{pendi} = \frac{1}{\omega_{\text{i0}}^2 - \omega^2 + i\omega\omega_{\text{i0}}/Q} \simeq -\frac{1}{\omega^2}. \tag{22}$$

In this document, we use the convention of calibration of a free mass at 1 Hz. Our reason for this convention is to simplify the calculation of the actuation coefficient by eliminating the need to use a pendulum resonance frequency and a quality factor for the resonance. All of our measurements are done at $\omega \gg \omega_0$ then we multiply our measurements by f^2 to scale down to 1 Hz. To convert between the traditional DC calibration and this free mass calibration at 1 Hz, simply multiply the DC calibration by the resonant frequency of the pendulum squared.

Similarly, we can also inject into the coil actuators on ifo:LSC-ETMi_EXC, reading back ifo:LSC-DARM_ERR. See Figure 14. This measurement can be scaled once the coils have been calibrated using either the "official" calibration method or using the photon calibrator (see Section 4.2).

Again, the loop algebra for the voice-coil excitation points gives the transfer functions give

$$\frac{\text{DARM\_ERR}}{\text{LSC-ETMX\_EXC}} = -\frac{\gamma(t)C(\omega,t_0)}{1+\gamma(t)G(\omega,t_0)} a_{\text{X}}\text{pendX} = -\frac{1}{R(\omega,t)} b_{\text{X}}\text{pendX} \tag{23}$$

for the X-arm voice-coil and

$$\frac{\text{DARM\_ERR}}{\text{LSC-ETMY\_EXC}} = \frac{\gamma(t)C(\omega,t_0)}{1+\gamma(t)G(\omega,t_0)} a_{\text{Y}}\text{pendY} = \frac{1}{R(\omega,t)} b_{\text{Y}}\text{pendY} \tag{24}$$

for the Y-arm voice-coil. Here, a_{X} and a_{Y} are the voice-coil calibration coefficients at 1 Hz.

We can take a transfer function measurement, say DARM_ERR/ETMX_CAL, and divide out the calibration coefficient (b_{X}) and free mass repsonse (pendX) to calculate the response function, $R(\omega, t)$. Figure 15 shows the result of this calculation using the data from Figure 13.

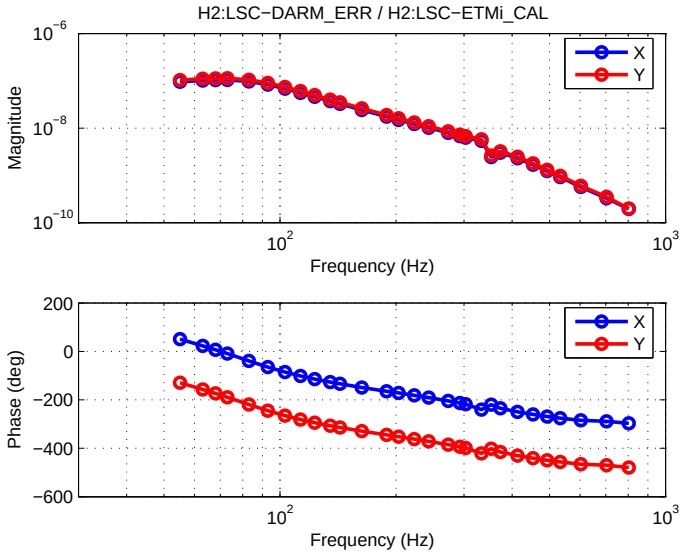

Figure 13: Uncalibrated transfer functions on H2 produced by the photon calibrators on November 8, 2006. The upper plot shows the magnitude (blue is the x-arm and red is the y-arm), the lower plot shows the phase with the x and y arms 180 degrees out of phase.

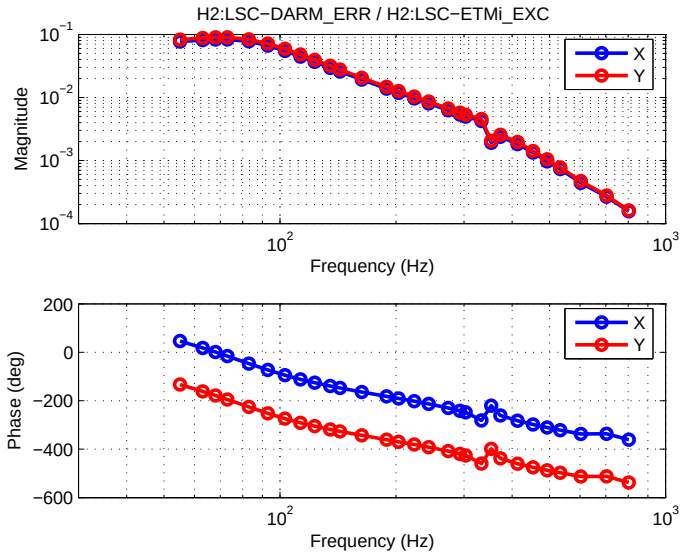

Figure 14: Uncalibrated transfer functions on H2 produced by the coil actuators on November 8, 2006. The upper plot shows the magnitude (blue is the x-arm and red is the y-arm), the lower plot shows the phase with the x and y arms 180 degrees out of phase.

4.2 ETM coil calibration

The photon calibrators inject directly onto the ETM while the coil actuators inject into the actuation path of the DARM loop after the output matrix but before the ETM digital actuation filters. Either the photon calibrator or the coil actuators can be used to measure the response function, but the coils must be calibrated prior to their use as a calibrator themselves. The typical calibration for the coil actuators is done via the "official" calibration method. Like the coils, the photon calibrators are also calibrated prior to use, but in a much simpilar manner (see Section 3.1).

By taking the ratio of photon calibrator transfer function and voice-coil actuator transfer function measure-

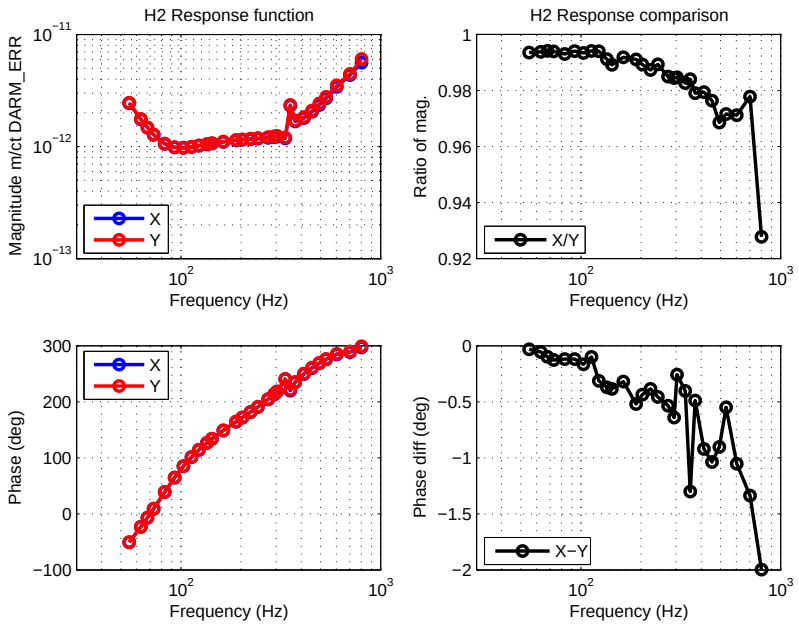

Figure 15: Response function of H2 produced by the photon calibrators. The upper left plot shows the magnitude (blue is the x-arm and red is the y-arm), the lower left plot shows the phase, the upper right shows a ratio of the magnitudes (x-arm/y-arm) and the lower right shows the difference in phase (x-arm minus y-arm).

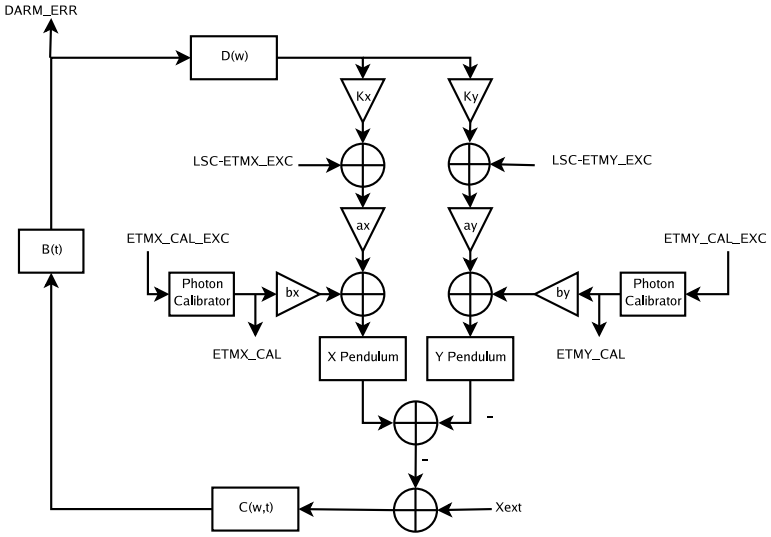

Figure 16: A schematic of the DARM servo loop with details identifying the injection points in the loop.

ments taken simultaneously or nearly-simultaneous, we can obtain the coil actuator calibration coefficients a_{X} and a_{Y} provided the photon calibrator calibration is known:

$$\frac{\text{ETMi\_CAL}}{\text{LSC-ETMi\_EXC}} = \frac{a_{\mathrm{i}}}{b_{\mathrm{i}}}. \tag{25}$$

where i = X, Y.

We can use the photon calibrators to calibrate the ETM voice-coil actuators in terms of meters moved per excitation count by driving an ETM sinusoidally at a given frequency with a photon calibrator, followed by driving the same ETM with the voice-coil actuators at the same frequency (or driving at the same time, but

separated by a small amount in frequency). In taking the ratio of the two transfer functions, the closed-loop gain, free mass transfer function of the ETM and sensing function of the interferometer divide out. The result is the ratio of the actuation coefficient of each method of excitation.

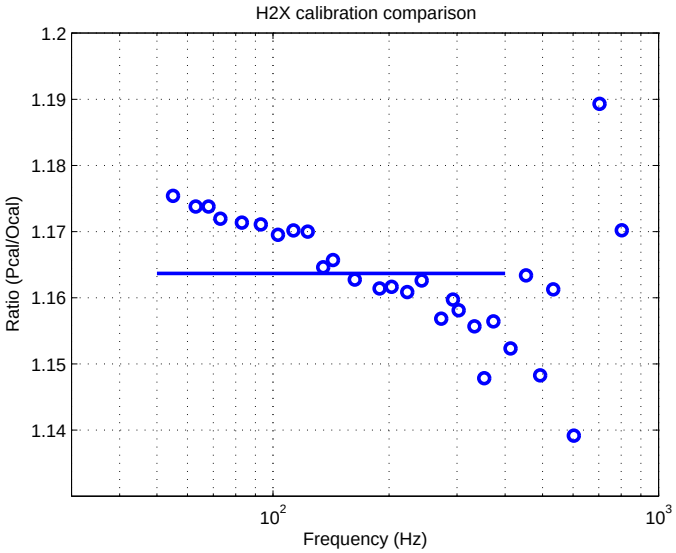

Figure 17: Ratio of H2 ETMX voice-coil calibration propagated to 1 Hz produced from the photon calibrators compared to the V2 calibration value.

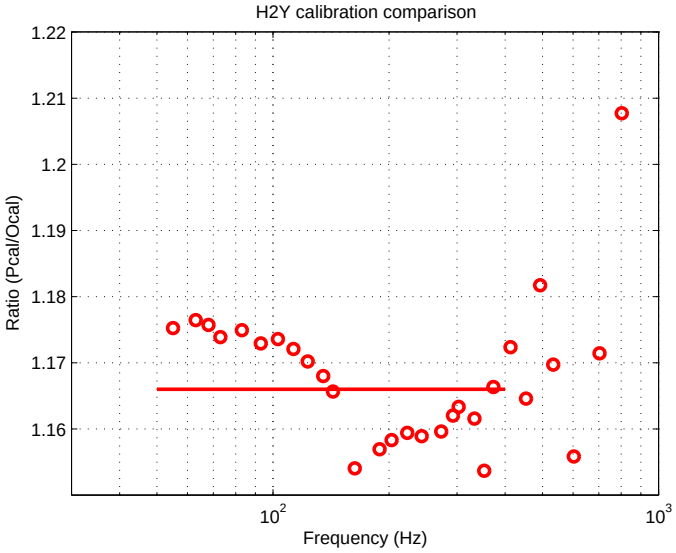

Figure 18: Ratio of H2 ETMY voice-coil calibration propagated to 1 Hz produced from the photon calibrators compared to the V2 calibration value.

4.3 Precision and reproducability of the photon calibrator

To understand how reproducable the photon calibrator measurements were, we ran an experiment with the photon calibrators and coils running for 5 hours on H2. The lines were offset from one another by 1.5 Hz all running near 803 Hz. By taking many FFT amplitudes from each of DARM_ERR, ETMi_CAL and ETMi_EXC

and taking the appropriate ratios, we can observe the calibration variation as a function of time. In this particular analysis we measured the calibration once per minute for 5 hours. This means the sampling rate for the measurement was 1/60 Hz. The signal-to-noise ratio (SNR) for the amplitude spectral density plots was roughly 10 for both the coil excitation and photon calibrator excitation.

The following plots show the results of this measurement on x-arm only. We had similar results on the y-arm. Figure 19 shows the time series of the coil calibration as a function of time. We made a histogram of the time series to find the mean and standard deviation of the measurement (Figure 20). This gives us a statistical error of $\sigma/\text{mean} \times 100 = 4$ percent. This can easily be improved by taking longer measurements that give better SNRs.

Next we take a power spectral density of this time series to understand any harmonic drifting effects that may occur over the 5 hour measurement time (see Figure 21). The plot has been zoomed in on the y-axis to show the frequency components above DC. There are no peaks in the spectrum that are significant above the noise. Note that the longer one measures the calibration line height ratio, the lower in frequency one moves along the x-axis of this plot.

Finally, to check that there was no correlation between the coil line and photon calibrator injected lines, we made a correlation plot. The result of this plot, Figure 22, shows that the correlation measure is very close to zero, meaning the correlation is very small.

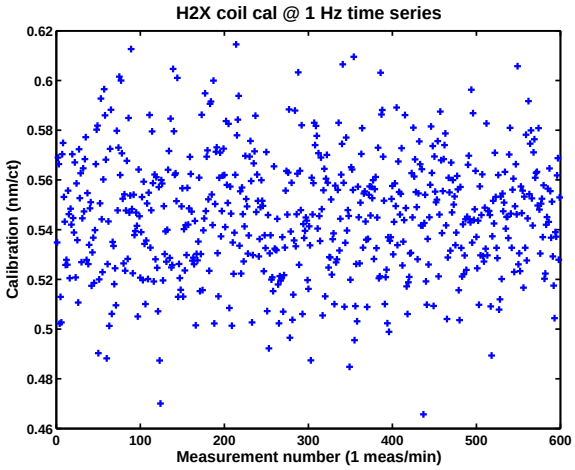

Figure 19: Time series of the effective calibration at 1 Hz for H2X as a free mass.

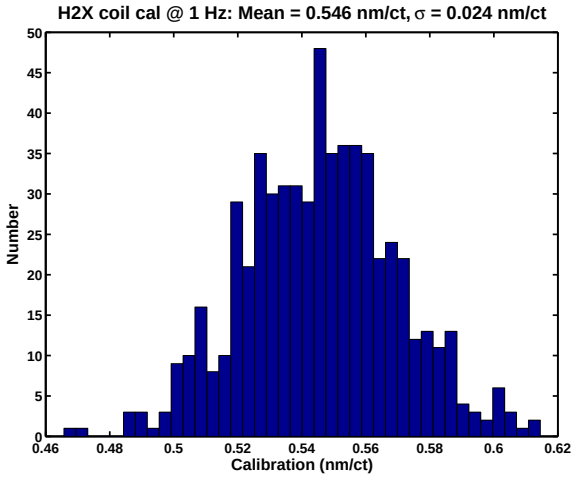

Figure 20: Histogram of the effective calibration at 1 Hz for H2X as a free mass.

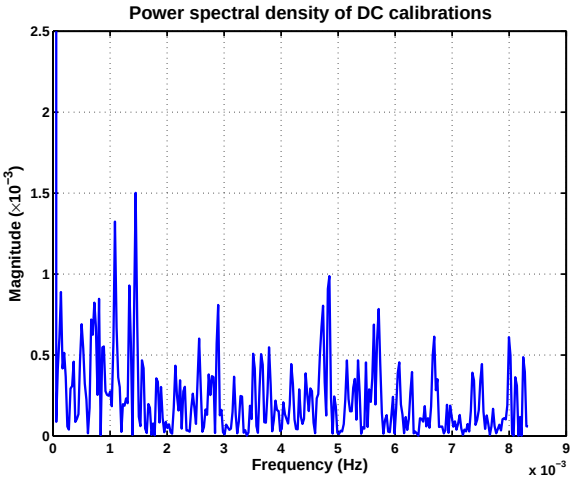

Figure 21: Power spectral density of the H2X calibration time series.

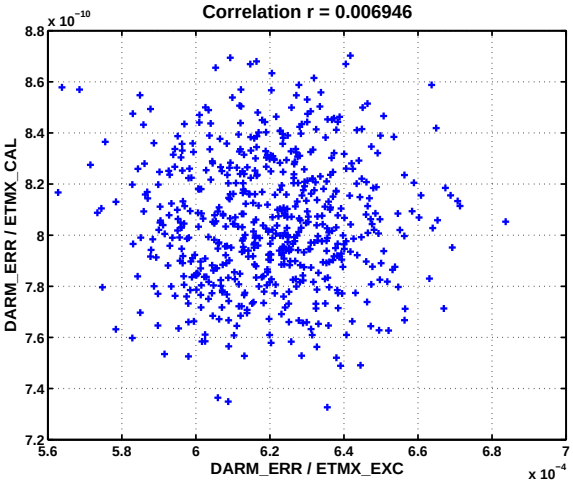

Figure 22: Correlation plot between coil excitation and photon calibrator excitation.

During the S5 run, we made several measurements on H2 with the photon calibrator. In Figure 23, we plot the calibration of the H2 y-arm coil actuator coefficient as produced by the photon calibrator. This covers two different optical configurations of the photon calibrator box. We conclude that a change in the configuration with a new photodiode calibration measurement does not affect the overall result of the photon calibrator.

4.4 Mirror rotation

In 2005, PK made a measurement to observe how an offset in the photon calibrator beam changes the calibration obtained. First, a calibration for how many knob turns of an optical mount it takes for the beam to scan left and right across the ETM. This was done with the interferometer out of lock so the photon calibrator beam could be viewed on the spool camera feed. Then, with the interferometer in full lock, a scan was made across the surface with the photon calibrator beam. The approximate beam position is noted and the measurement number is given in Figure 24.

The slope of a fit to this line of points given the ETM mass, moment of inertia, and photon calibrator beam offset gives the average offset of the main interferometer beam. From this measurement we determined the main interferometer beam was offset 2.8 mm to the left of center. No measure of the vertical offset was made, but a simlar procedure would yield a measure of the vertical offset to the main interferometer beam.

This experiment validates the correction term used in Equation 15 due to off-centered beams.

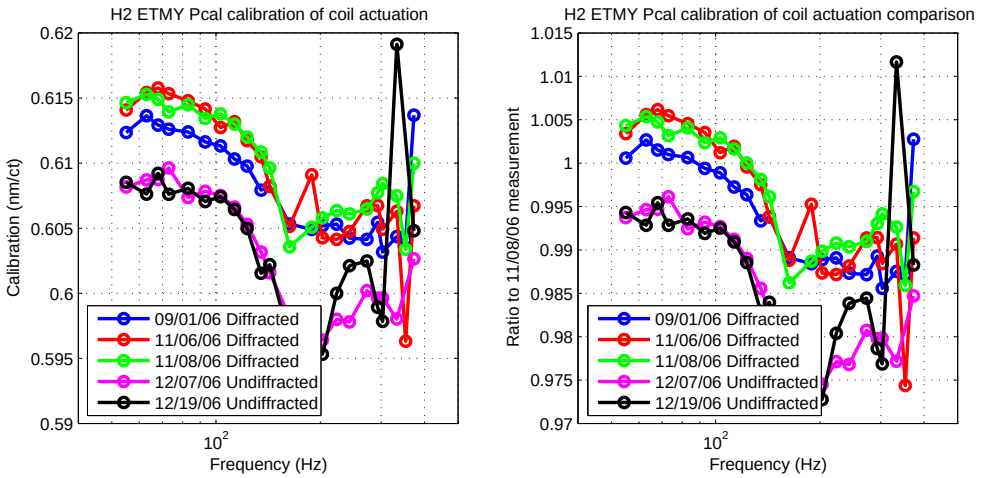

Figure 23: Several measurements made with the photon calibrators over a three month period on the H2 interferometer showing agreement to better than 2% up to $\sim$400 Hz.

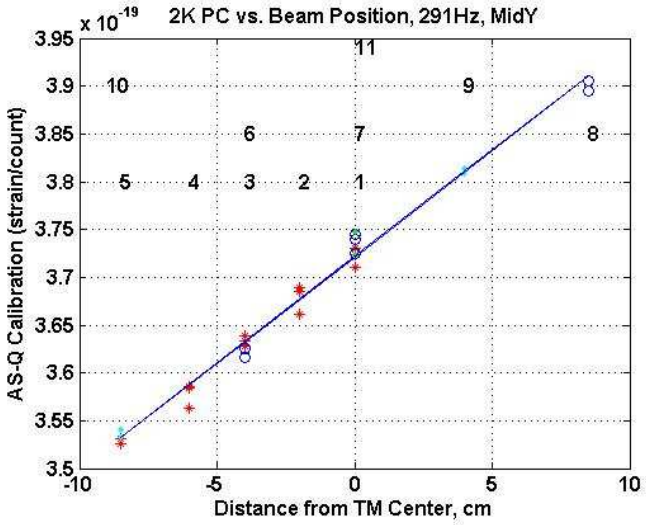

Figure 24: Experimental verification of the correction term in equation 15 due to off-centered beams. The x-axis shows approximate position of the photon calibrator beam relative to the center of the test mass, and the y-axis shows the magnitude of the response function $R(\omega)$. The fit to experimental data indicates that the main interferometer beam was offset by 2.8 mm to left of center. The measurements were made on the Y-arm of the H2 interferometer.

4.5 Correction for comparing lines separated by small amount in frequency

When measuring the calibration of the coils using the photon calibrator by *simultaneously* driving with the coils and photon calibrator, but separated in frequency, there is a slight correction due to frequency dependence of the free mass respsonse and the response of the interferometer. We calculate this correction factor from the V2 version of the calibration model.

==Put in the plot for the correction factor==

For our measurements on H2 for 5 hours at about 803 Hz, the correction is $\sim$ 1 percent.

4.6 Calibration discrepancy summary

We have therefore performed a measurement of the absolute coil actuation calibration coefficient for an end test mass (ETM) using the photon calibrator. This value can then be compared to conventional measurements. The results are presented in Table 5. The Hanford detectors show agreement between the photon calibrators and the conventional calibration of 16 to 17 percent, while the L1 detector shows agreement between 8 and 14 percent.

Table 5: Summary of photon calibrator discrepancies.

Optic	Date	Pcal ETM Cal	V2 Coil ETM Cal	Pcal / Coil
H1 ETMX	N/A	N/A	0.470×10^{-9} m/ct	N/A
H1 ETMY	Sept. 28, 2006	0.570×10^{-9} m/ct	0.489×10^{-9} m/ct	1.17
H2 ETMX	Nov. 8, 2006	0.561×10^{-9} m/ct	0.482×10^{-9} m/ct	1.16
H2 ETMY	Nov. 8, 2006	0.610×10^{-9} m/ct	0.523×10^{-9} m/ct	1.17
L1 ETMX	March 16, 2007	0.291×10^{-9} m/ct	0.255×10^{-9} m/ct	1.14
L1 ETMY	March 16, 2007	0.258×10^{-9} m/ct	0.239×10^{-9} m/ct	1.08

5 Uncertainties

We analyze the systematic errors using the equation

$$\left(\frac{\Delta x}{x}\right)^2 = \left(\frac{\Delta P_0}{x}\frac{\partial x}{\partial P_0}\right)^2 + \left(\frac{\Delta \cos\theta}{x}\frac{\partial x}{\partial \cos\theta}\right)^2 + \left(\frac{\Delta M}{x}\frac{\partial x}{\partial M}\right)^2 + \left(\frac{\Delta a}{x}\frac{\partial x}{\partial a}\right)^2 + \left(\frac{\Delta b}{x}\frac{\partial x}{\partial b}\right)^2 \quad (26)$$

where $\Delta x/x$ is the fractional change in the amplitude of the displacement due to the systematic errors, ΔP_0 is the change in power, $\Delta \cos\theta$ is the change in the cosine of the angle, ΔM is the change in mass of the ETM, Δa is the change in the photon calibrator beam offset and Δb interferometer beam offset from the center of mass.

5.1 Photodetector Calibration Factor

We calibrate the photodetector with Ophir power meters using a thermal head (10A). The manufacturer quotes a calibration uncertainty of 3 percent for a properly calibrated thermal head. Our units are regularly sent back to Ophir for recalibration approximately once per year. The initial calibration of the photodetector is therefore given a 3 percent uncertainty.

5.2 Viewport reflectivity

The viewport reflectivity is measured using an Ophir power meter with a low power silicon photodiode head (PD300). Ophir quotes a calibration uncertainty of 5 percent for a calibrated head with the neutral density filter removed. We also must set power meter to measure the photon calibrator wavelength of 1047 nm. We measure the maximum of the viewport reflectvities to be less than 8 percent (measured at the 1064 nm wavelength setting) corresponding to less than 6.4 percent when measured at the 1047 nm wavelength setting.

A 5 percent error on a reflection of 6.4 percent is a 0.3 percent uncertainty (0.5 percent when including the error on measuring the incident power with the 10A thermal head).

5.3 ETM reflection

The ETM transmission is measured to be 0.03 percent of the total incident power. Assuming minimal absorption in the substrate, the reflected power is 99.97 percent of incident power. An error of 5 percent on the measure of transmitted power gives a negligable change in the ETM reflection coefficient. We therefore ignore the contribution of this error.

5.4 Angle of incidence

(Maximum change in angle of incidence 2 degrees?)

5.5 Mass of the optic

The error on this value is small, given the results of a calculation of the mass of an input test mass (ITM) and an actual massing of the optic. We assign an error of 0.1 percent to the error in the value of the mass of the ETM.

5.6 Photon calibrator spot position

We estimate that we know the photon calibrator spot position within 5 mm of its actual location on the optic. This estimate comes from the spool camera images. However, we believe that the photon calibrator beam is centered on the H2 and L1 interferometers meaning that $a = 0$. H1 has baffle supports that occlude the center of the optic. We estimate the position of the x-arm to be ?? and the y-arm to be 1.6 cm(?).

5.7 Interferometer beam position

The maximum offset of the interferometer beam is... (2 cm?), and we assume that we can measure the beam position to within 5 mm.

5.8 Statistical error

Statistical errors arise in the calibration due to random fluctuations in laser power and instrument sensitivity. These errors can be reduced by increasing the SNR of the measurement. As an example, the 5 hour measurements made on H2 had a statistical error of 4 percent. The error can be reduced at the cost of an increase in measurement time.

5.9 Summary

For systematic uncertainties,

$$\left(\frac{\Delta x}{x}\right)^2 = \left(\frac{\Delta P_0}{P_0}\right)^2 + \left(\frac{\Delta \cos\theta}{\cos\theta}\right)^2 + \left(\frac{\Delta M}{M(1+abM/I)}\right)^2 + \left(\frac{bM\Delta a}{I(1+abM/I)}\right)^2 + \left(\frac{aM\Delta b}{I(1+abM/I)}\right)^2 \tag{27}$$

Therefore, putting in the values and assuming that $a = 0$ cm, $b = 2$ cm, $M = 10.35$ kg, and $I = 0.0491\text{kg}\cdot\text{m}^2$

$$\begin{aligned}\left(\frac{\Delta x}{x}\right)^2 &= (0.03+0.005)^2 + \left(\frac{\cos 11.6^\circ - \cos 9.6^\circ}{\cos 9.6^\circ}\right)^2 + (0.001)^2 + \left(\frac{0.02\cdot 10.35\cdot 0.005}{0.0491}\right)^2 \\ \frac{\Delta x}{x} &= 0.041.\end{aligned}$$

For $a = 1.6$ cm and $b = 2$ cm, $\Delta x/x = 0.044$. More likely, $b \simeq 0$ which means that $\Delta x/x = 0.036$ for $a \simeq 0$.

Therefore, our systematic error is, conservatively, 5 percent and the statistical error is 4 percent. As we have stated previously, the statistical error can be reduced by increasing the SNR of a measurement.

6 Conclusion

Photon calibrators provide an independent calibration of LIGO's three gravitational wave detectors. Agreement with the conventional calibration is at the 16-17 percent level for the two Hanford detectors, and at the 8-14 percent level at Livingston. Intrinsic ncertainty in these results at the 1σ level is, conservatively, 5 percent for the six LIGO photon calibrator units. Since the uncertainty on the conventional calibration is estimated to be $\sim$5%, there is an unresolved systematic discrepancy. In the future, we hope to resolve the discrepancy.

Finally, we note that the photon calibrators have the potential for measuring phase lags in the detectors' control systems, and for injecting calibrated hardware waveforms into gravitational wave data. Photon calibrator hardware injections could be useful in realistic blind data analysis tests.

Acknowledgements

We are indebted to many of our colleagues for frequent and fruitful discussions. In particular we would like to thank David Barker, GariLynn Billingsley, Douglas Cook, Valera Frolov, Gabriela Gonzalez, Mark Guenther, Michael Landry, Douglas Lormand, Richard McCarthy, Brian O'Reilly, Keith Riles and Rusyl Wooley for valuable suggestions and support.

A Photodetector calibration

Provided there are no adjustments to the optical configuration of the photon calibrator, the photodetector calibration should remain constant with time. We made numerous calibrations at LLO in March of 2007 to check the reproducability and stability of the photodetector calibration.

==Add Rick's plots==

B Viewport reflection

EG and RS observed two spots when the angle of incidence was increased from the nominal 9 degrees angle of incidence (see LHO elog 22 December 2006, following section). In each spot (at higher than normal angle of incidence) the reflection coefficient was 4.4 percent. The viewport used for this measurement was the output viewport of the H2 ETMX optical lever laser. However, it has similar reflection properties as the 7 percent reflecting viewports for the photon calibrators.

C ETM reflection

EG and RS measured the ETM reflectivity in situ using a photon calibrator aimed through an optical lever laser viewport (see LHO elog from 10 October 2006 and 22 December 2006).

```
Today, we utilized the spare photon calibrator laser (1047 nm) to
measure the optical lever output window reflectivity.

Here are the numbers:
Today's measurements (using Ophir power meter #4, solid state
detector without the filter)-
incident power = 8.85 mW
reflected power = 0.502 mW
reflectivity = .502/8.52 -> 7.4%

Earlier measurements:

Power to input viewport (trial 1): 392 mW
Power out of the output viewport (trial 1): 345 mW
(overall efficiency = 345/392 -> 88.0%)

Power to input viewport (trial 2): 387 mW
Power out of the output viewport (trial 2): 342 mW
(overall efficiency = 342/387 -> 88.4%)

Power reflecting off the input viewport: 27.0 mW
reflectivity = 27/((387+392)/2) -> 6.9%

We expect the test mass reflectivity to be 99.97%

Thus we would expect the transmission efficienty to be:

0.931 * 0.9997 * 0.926 = 86.2%

We measured closer to 88%. This is likely due to measuring the output
window reflectivity at closer to normal incidence than during the overall
transmission measurement. Today, we purposely increased the incidence
angle to about 11 deg. so that we could see two distinct reflected spots.
At this angle, the viewport reflectivity was 0.391/8.85 -> 4.4%. The
incidence angle for the photon calibrators is about 9.1 deg. Using the 11
deg. reflectivity, the expected overal transmission would be
```

```
0.931 * 0.9997 * 0.956 = 89.0%

Bottom line - there is no anomalous loss of power in the photon
calibrator propagation, at least for MidX.
```

D Angle of incidence

The angle of incidence is determined from the ISC drawing LIGO-D970220-C-D. The distances are calculated from center of the viewport window to the center of the ETM HR surface.

E ETM mass

PK's Matlab script for determining mirror mass:

```
% From a Gari e-mail:
%
% Finally... SPETM01
% Diameter 249.848 mm
% Thickness 99.126 to max sharp corner\
% Wedge  1.968 Degrees
% Side one chamfer 1.78 mm
% Side two chamfer 1.98 mm

% from coc as built
% BLANKS
% ETM01  25.677 x 10.901
% ETM02  25.684 x 10.889
%
% SPETM03  25.684 x 10.901
% SPETM05  25.671 x 10.896
% SPETM06  25.054 x 9.995
% SPETM07  25.027 x 10.002

% POLISHED SUBSTRATES
% ETM01  25.075 x 9.963
% ETM02  25.088 x 9.993
%
% SPETM03  25.061 x 9.9863
% SPETM05  25.0482 x 9.9977
% SPETM06  25.054 x 9.995
% SPETM07  25.027 x 10.002

dens = 2.201;                %Suprasil family (we have 312)
% L = 10;                    %test mass cylinder length in cm
% r = 12.5;                  %test mass radius
%
%
% L = 9.9126
% r = 24.9849/2
%
% % L = 10.901
% % r = 25.677/2
%
% ang = 2.0;                 %test mass wedge in deg
% tmChamferLeg = 0.2;        %test mass chamfer leg length, cm
%
```

```
%
% mnom = pi*r2*L*dens         %nominal mass not considering chamfer
%
% angrad = ang/180*pi;                    %test mass wedge in radians
% delm = pi*(12.52)*(sin(angrad)*25)/2   %mass of removed wedge material
% mcham = 2e-2 * pi *25 * dens * 2       %mass of removed chamfers - 2 mm
 %both faces
% m = mnom - delm - mcham                %net mass of test mass in grams




%test mass chamfer leg length, cm, rounded to same value for all ETMs


% POLISHED SUBSTRATES
% ETM01 || 10.346 || 25.075  ||  9.963  || 2d00m  || 0.216 || 0.193 ||
% ETM02 || 10.388 || 25.088  ||  9.993  || 2d00m  || 0.217 || 0.226 ||
%
% SPETM03 || 10.363 || 25.061  ||  9.9863 || 1.989d || 0.212 || 0.180 ||
% SPETM05 || 10.365 || 25.0482 ||  9.9977 || 1.983d || 0.199 || 0.189 ||
% SPETM06 || 10.372 || 25.054  ||  9.995  || 1d58m  || 0.198 || 0.203 ||
% SPETM07 || 10.353 || 25.027  || 10.002  || 1d59m  || 0.193 || 0.211 ||

% results from running this script
% M =
%   10.34569803251292
% M =
%   10.38758907443100
% M =
%   10.36289016520503
% M =
%   10.36508409558616
% M =
%   10.37171099757591
% M =
%   10.35337876052679


dVect = [ 25.075 , 25.088 , 25.061 , 25.0482 , 25.054 , 25.027 ];
lVect = [ 9.963 , 9.993 , 9.9863 , 9.9977 , 9.995 , 10.002 ];
angVect = [ 2, 2, 1.989, 1.989, 1 + 58/60, 1+59/60 ];
chmf1Vect = [ 0.216 , 0.217 , 0.212 , 0.199 , 0.198 , 0.193 ];
chmf2Vect = [  0.193 ,  0.226 , 0.180 , 0.189 , 0.203 , 0.211    ];


% Finally... SPETM01
% Diameter 249.848 mm
% Thickness 99.126 to max sharp corner\
% Wedge  1.968 Degrees
% Side one chamfer 1.78 mm
% Side two chamfer 1.98 mm

%%%%%%%%%%%%%%%%%%%%%%%%%%%%%%%%%%%%%%%%%%%%%%%%%%%%%%%%%%%%%%%%%%%%%%%
%calculation of mass of ITMx
```

```
%expected uncertainty contribution ~1%
%
dens = 2.201;

mVect = [];
for i = 1 : 6

tmLength = lVect(i);
tmRadius = dVect(i)/2;
tmWedgeAngle = angVect(i);
tmChamferLeg1 = chmf1Vect(i);
tmChamferLeg2 = chmf2Vect(i);


% tmLength = 9.963
% tmRadius = 25.075/2
% tmWedgeAngle = 2
% tmChamferLeg = 0.2;

% tmLength = 10
% tmRadius = 25/2

% tmLength = 9.9126
% tmRadius = 24.9848/2

angrad = tmWedgeAngle/180*pi;
%nominal mass not considering chamfer
mnom = pi * tmRadius2 * tmLength * dens;
%mass of removed wedge material
delm = pi * tmRadius2 * (tan(angrad) * 2 * tmRadius) / 2 * dens;
%mass of removed chamfers
mcham1 = (tmChamferLeg12 / 2) * pi * 2 * tmRadius * dens;
mcham2 = (tmChamferLeg22 / 2) * pi * 2 * tmRadius * dens;
%net mass, g
m = mnom - delm - mcham1 - mcham2;
%net mass, kg
M = m/1000

mVect = [mVect M];

end

mean(mVect)
std(mVect)



% tmLength = 9.963
% tmRadius = 25.075/2
% tmWedgeAngle = 2
% tmChamferLeg = 0.2;

% tmLength = 10
% tmRadius = 25/2

% tmLength = 9.9126
```

```
% tmRadius = 24.9848/2

tmLength = 10.901
tmRadius = 25.677/2

angrad = tmWedgeAngle/180*pi;
%nominal mass not considering chamfer
mnom = pi * tmRadius2 * tmLength * dens;
%mass of removed wedge material
delm = pi * tmRadius2 * (tan(angrad) * 2 * tmRadius) / 2 * dens;
%mass of removed chamfers
mcham1 = (tmChamferLeg12 / 2) * pi * 2 * tmRadius * dens;
mcham2 = (tmChamferLeg22 / 2) * pi * 2 * tmRadius * dens;
%net mass, g
m = mnom - delm - mcham1 - mcham2;
%net mass, kg
M = m/1000

mVect = [mVect M];
```